Applications of oil and gas interpretation and modeling practices to windfarm soil characterization

Leon Barens[1], Khalid Tarek[1], Julien Lalanne[2] and Eric Cauquil[3]

ABSTRACT

The growing demand for renewable energy has been a driving force behind the rise of windfarms, whose development now increasingly relies on data acquisition methods similar to those used in oil and gas projects. Although the nature of these data collected may be similar, their objectives differ significantly. In windfarm energy projects, understanding soil strength, particularly the small-strain shear modulus (G_{max}), is essential for enhancing turbine foundation design. G_{max} can be derived from shear wave velocity, if the bulk density is known.

To assess soil strength, techniques traditionally used in hydrocarbon reservoir characterization and modeling can be effectively adapted. High-resolution 2D seismic data are interpolated into a 3D grid, allowing the application of modern interpretation techniques. Geotechnical well logs are projected onto crossplots and used to classify the subsurface into Soil Behaviour Types (SBTs), analogous to facies in reservoir studies. Machine learning techniques are then applied to 2D seismic data to generate a channel density map, which helps constrain the 3D modeling of subsurface channels. This integrated workflow produces a suite of 3D SBT models in which shear wave velocity is co-simulated. From these models, the small-strain shear strength can be estimated, along with its associated uncertainty, assuming density is known.

KEYWORDS

Windfarm, turbine foundation, soil behaviour types, uncertainty assessment, reservoir characterization

INTRODUCTION

Wind and solar energy are key components of renewable power, both offering relatively low carbon emissions. Wind energy, specifically, is harnessed through the development of windfarms, which involve the optimal placement of multiple wind turbines within a designated lease area. This lease must be located in a region with consistent wind resources and proximity to electricity consumers. Offshore sites are especially well-suited for windfarm development due to their favorable wind conditions and spatial availability. Within an offshore lease, the turbine placement is optimized to maximize energy yield based on prevailing wind directions (Cazzaro et al., 2022). Each wind turbine consists of a foundation anchored into the seabed, and a pylon supporting the structure. In European offshore windfarms, monopiles are the most common type of foundation (Vieira et al., 2019). These are large steel cylinders, typically 4 to 8 meters in diameter, driven deep into the seabed. As turbine sizes increase, so too must the dimensions of their supporting monopiles.

Turbine foundations must be engineered to withstand cyclic loading from wind and waves. A critical design factor is the structure's natural (eigen) frequency, which must fall outside the excitation frequencies generated by environmental forces and turbine operation, such as rotor rotation and blade passage past the pylon (Lombardi et al., 2013). To calculate these eigenfrequencies, Finite Element Modelling (FEM) can be employed, although it is computationally intensive (Murphy et al., 2018). A more commonly used and computationally efficient method is the Winkler foundation model, originally developed in 1867 (Arany et al., 2017). In this approach, the turbine and foundation are treated as a rigid beam subjected to cyclic forces. The interaction of the foundation with the soil is modelled as a set of independent or uncoupled springs, each corresponding to different small-scale shear strengths of the soil formations (Damgaard et al., 2014), as illustrated in Figure 1. The objective of foundation design is to ensure that the system's natural frequencies are kept clear of the excitation ranges, thereby enhancing structural stability and longevity.

In oil and gas field development, reservoir modeling serves to capture subsurface heterogeneities within a gridded framework to forecast hydrocarbon production. These models aim to optimize resource extraction by

[1]TotalEnergies, OneTech/R&D/Sismage, Pau, France; [2]TotalEnergies, OneTech/TL/POW/Wind, Pau, France.
[3]TotalEnergies, OneTech/TL/TEC/GEO, Paris, France. | http://dx.doi.org/10.63606/ghz-0972-7132-2-2025-13

Emails: leon.barens@totalenergies.com; khaled.tarek@external.totalenergies.com; julien.lalanne@totalenergies.com; eric.cauquil@totalenergies.com

minimizing the number of wells required, targeting hydrocarbon reservoirs typically located between 1,000 and 6,000 m in depth. This model is constructed through comprehensive analysis of available data, including seismic interpretation, laboratory measurements, and specialized studies, to enable the simulation and prediction of fluid flow through the reservoir.

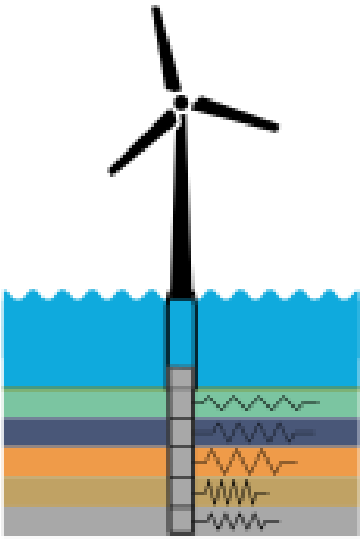

***Figure 1**: Schematic of a wind turbine, consisting of a foundation up to the seabed, a transition piece and a pylon holding the turbine at the top. The foundation is piecewise coupled with the soil through springs in the Winkler solid beam method. This method aims to model the eigen frequency of the structure.*

In contrast, windfarm developments require detailed characterization of the lease area soil, specifically in terms of small-strain shear strength (G_{max}), to support foundation design. During the turbine design phase, predictions are made about the fatigue life of the turbine structures under cyclic loading, based on assumptions regarding both soil strength and environmental conditions.

While the objectives of oil and gas and wind energy developments differ, both rely on similar types of subsurface data, primarily obtained through borehole sampling and seismic surveys. Our approach leverages established interpretation and modeling techniques from the hydrocarbon sector, applying them to windfarm data to generate a suite of models that characterize the small-strain shear strength of the soil. However, due to inherent differences between hydrocarbon reservoir and geotechnical datasets, the latter must be adapted to ensure compatibility with reservoir modeling workflows.

By integrating these adapted datasets into hydrocarbon-derived modeling frameworks, we construct shear wave velocity models from the windfarm data. When combined with soil bulk density information, these models allow us to derive the small-strain shear strength (G_{max}) of the subsurface soil. This family of models not only supports foundation design by providing critical soil strength information, but also highlights areas of high uncertainty, helping to guide future data acquisition efforts.

Our study is structured in three phases. We begin by analyzing the key differences between datasets collected for hydrocarbon reservoir and windfarm developments. After this, we interpret and analyze the seismic and borehole data acquired over a windfarm lease area. Finally, we prepare the data for modeling and construct the shear wave velocity models.

The outcomes of each phase are summarized in the conclusions.

DIFFERENCES BETWEEN THE DATA ACQUIRED FOR HYDROCARBON AND WINDFARM DEVELOPMENTS

In hydrocarbon development the wells are primarily drilled to optimise production of hydrocarbons. During the early stages of exploration and development, data acquisition is focused on characterizing the reservoir. Along the borehole wall, various measurements and samples are collected to determine the physical properties of both the geological formations and the fluids encountered. Occasionally, cores are retrieved to provide a more detailed understanding of the geological setting and to enable further reservoir property analysis.

In contrast, offshore windfarm developments rely on systematic geotechnical investigations, with the Cone Penetration Test (CPT) being a key method. A CPT involves pushing an instrumented cone vertically into the ground. As the cone penetrates the soil, three primary measurements are recorded: the *tip resistance* (q_c), representing the force required to penetrate the cone tip into the soil; the *sleeve friction* (f_s), indicating the frictional resistance encountered by the sleeve, and the *pore pressure* (u_2), the pressure measured at a specific

© SPG India. All rights reserved.

location on the cone, recorded continuously. These measurements are used to derive normalized cone parameters, following the methodology of Robertson (2009). In some cases, shear wave velocity (V_S) is also measured using a Seismic Cone Penetration Test (SCPT), where a surface-triggered shear wave source allows V_S measurements to be taken at regular intervals during penetration. These CPT and SCPT tests are often complemented by drilled boreholes, which provide core samples for sedimentological descriptions and detailed geotechnical laboratory analyses.

In oil and gas reservoir characterization, dedicated 3D seismic datasets are the industry standard, enabling detailed imaging of the subsurface across a range of depths. These datasets typically operate within a seismic bandwidth of 10 to 70 Hz and are processed using advanced techniques to resolve structural and stratigraphic features.

In contrast, offshore windfarm development commonly utilizes 2D Ultra High Resolution Seismic (UHRS) data for site characterization. UHRS data have a much higher frequency bandwidth, ranging from 200 to 1,000 Hz, allowing for greater resolution of near-surface features. UHRS lines are acquired in dense grids, with line spacing typically between 50 and 250 m, while perpendicular tie lines are spaced more broadly to provide structural context.

HYDROCARBON INTERPRETATION TECHNIQUES APPLIED ON WINDFARM DATA

Despite the distinct differences in the objectives of oil and gas versus offshore windfarm developments, there are clear opportunities to adapt, and leverage established oil and gas practices for use in offshore wind projects, particularly in the characterization of shallow soil conditions critical for foundation installation. In offshore wind, a typical soil facies model extends to approximately 100 m below the seabed. Both conventional and novel tools have been demonstrated to construct ground models that support the engineering of monopile foundations.

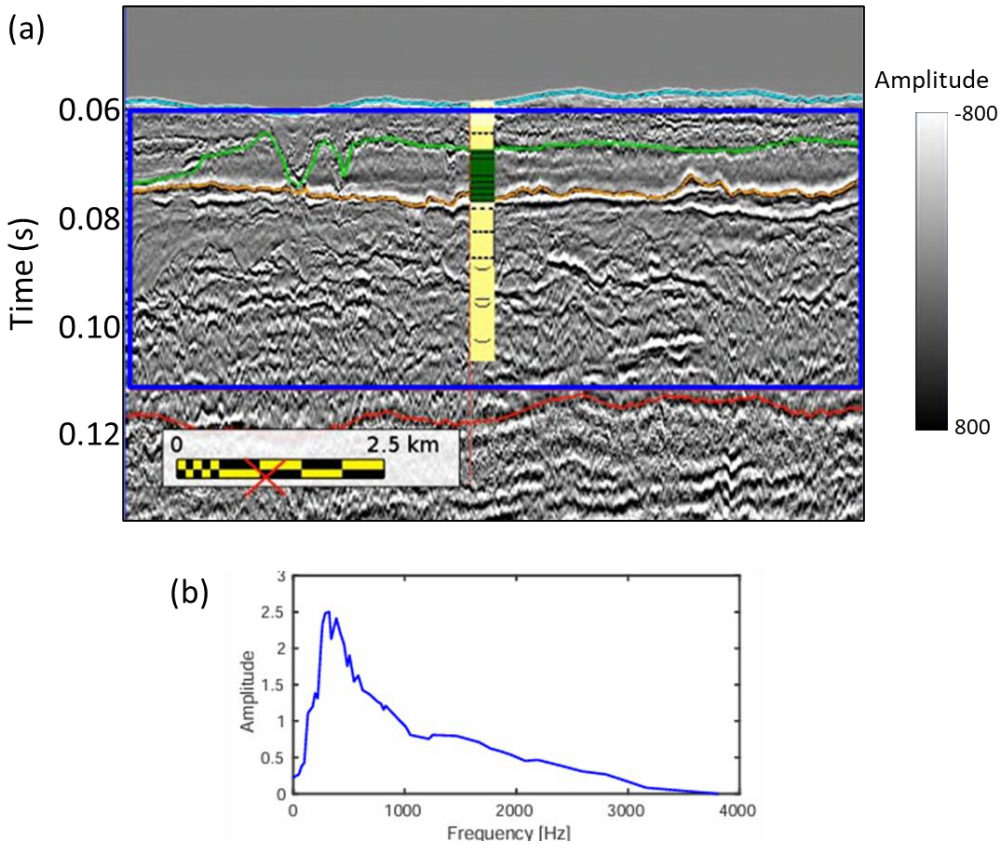

***Figure 2**: (a) A 2D Ultra High Resolution Seismic (UHRS) line through a borehole location. The blue box indicates the area used for generating the frequency spectrum shown in (b). Due to the high frequency content of the data, detailed seismic interpretations are made from these data above the first seabed multiple, red horizon.*

© SPG India. All rights reserved.

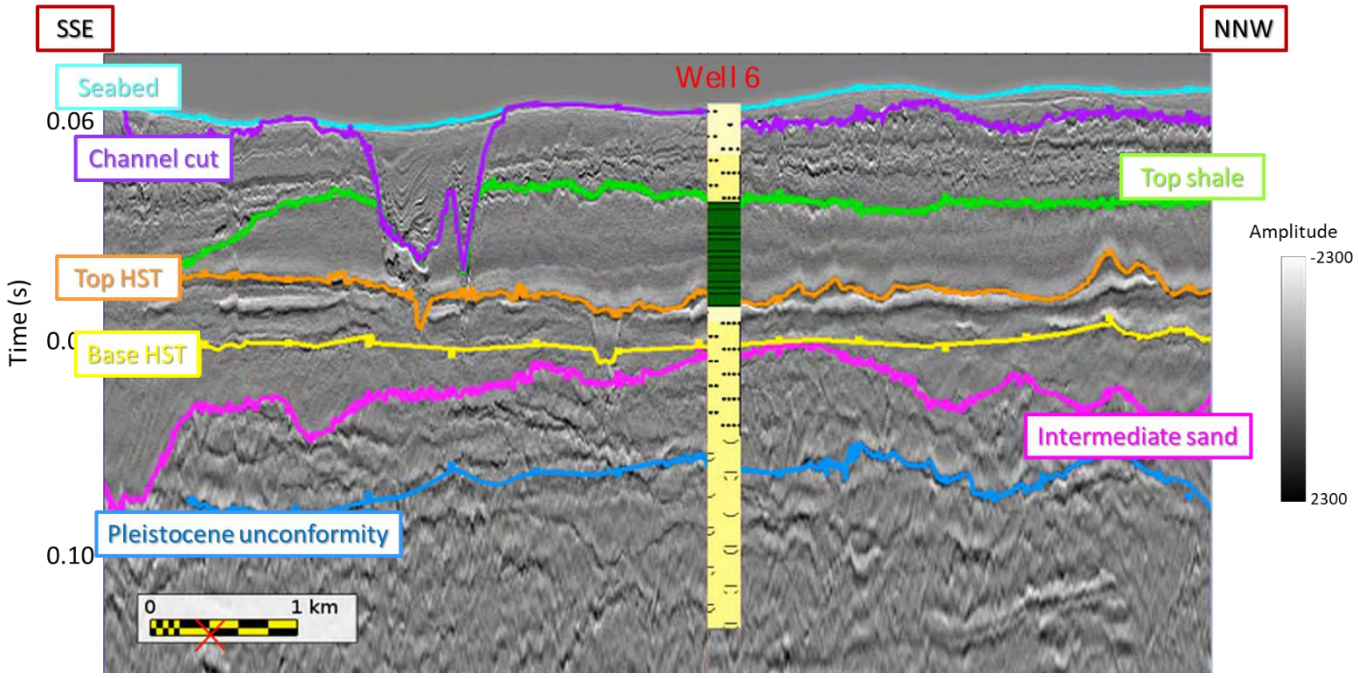

***Figure 3**: A 2D seismic line with the interpreted horizons and a stratigraphic column extracted at a borehole location. The horizons follow the regional interpretation of the area, Pleistocene Unconformity and the High Stand Systems Tract (HST). Local horizons are picked from the intersections of the well with the seismic data. These horizons are used to construct a 3D stratigraphic model.*

These methods are demonstrated using a dataset acquired specifically for this purpose, which includes a 2D UHRS survey. This survey was conducted using a dense acquisition grid: 2D seismic lines were spaced at 150 m, with perpendicular crosslines acquired every 500 m. Data were sampled at a temporal resolution of 0.125 milliseconds, with a trace interval of approximately 1.5 m. A sparker source was employed, producing a high-frequency bandwidth ranging from 150 Hz to 4,000 Hz. Following acquisition, the seismic data underwent a processing workflow, producing a final time-migrated stacked section along with an associated seismic velocity model. Figure 2 shows an example of the processed data along with the extracted bandwidth.

Geotechnical well data were collected at a total of 10 locations within the lease area. Of these, Seismic Cone Penetration Tests (SCPT) were performed at 4 locations, while standard CPTs were conducted at the remaining 6. At each site, boreholes were also drilled to retrieve soil samples, which were subsequently analyzed in the laboratory to determine key geotechnical parameters, including soil density.

Seismic interpretation

On the 2D seismic lines, stratigraphic horizons were interpreted through guidance by the regional burial history. To enhance accuracy of these interpretations, the 2D UHRS velocity model was calibrated using borehole velocity data, enabling time-domain correlation between seismic and borehole interpretations. Stratigraphic markers were identified based on regional geological descriptions and geotechnical log data, enabling the recognition of key depositional events. Interpretations are limited to depths above the first seabed multiple, beyond which seismic signals become ambiguous and interpretations increasingly speculative; therefore, no analysis has been conducted below this boundary.

Figure 3 shows a 2D seismic line with interpreted horizons intersected by a borehole. Based on regional stratigraphy, the top and base of a Highstand Systems Tract (HST) sand package were interpreted throughout the dataset. This sand package serves as a boundary between the underlying Pleistocene sands and the overlying shale-dominated estuarine environment,

© SPG India. All rights reserved.

which includes channel incisions formed during a sea-level regression.

On top of this shale and channel cut dominated package, a sequence of sand dominated transgressive channels are observed. Just beneath the seabed, a transgressive Holocene sand fan is interpreted, with thickness increasing toward the southeast of the study area. Beneath the HST sand package lies a succession of Pleistocene sands, which rest atop the Pleistocene Unconformity. Below this unconformity, well-consolidated or lithified coastal plain deposits are encountered. These interpreted horizons form the basis for constructing a comprehensive 3D stratigraphic model of the region.

Given the impracticality of manually identifying individual channels within the progressive channel deposits on the 2D seismic dataset, a semantic segmentation U-Net model was implemented to assist with interpretation. Initially, channel features were manually labeled on a segment of a 2D line and used to train the deep learning model. During training, the model optimized its predictions by minimizing the cross-entropy loss between its output and the provided labels.

Once trained, the network was applied across all 2D seismic lines to predict channel locations, as illustrated in Figure 4. Using the bounding horizons of the progressive channel deposits, a relative channel density profile was generated along each line, considering only channels with a prediction probability exceeding 0.6. These density profiles were then interpolated between seismic lines and smoothed to produce a channel density map, which highlights the preferential pathways of channel migration within the depositional sequence.

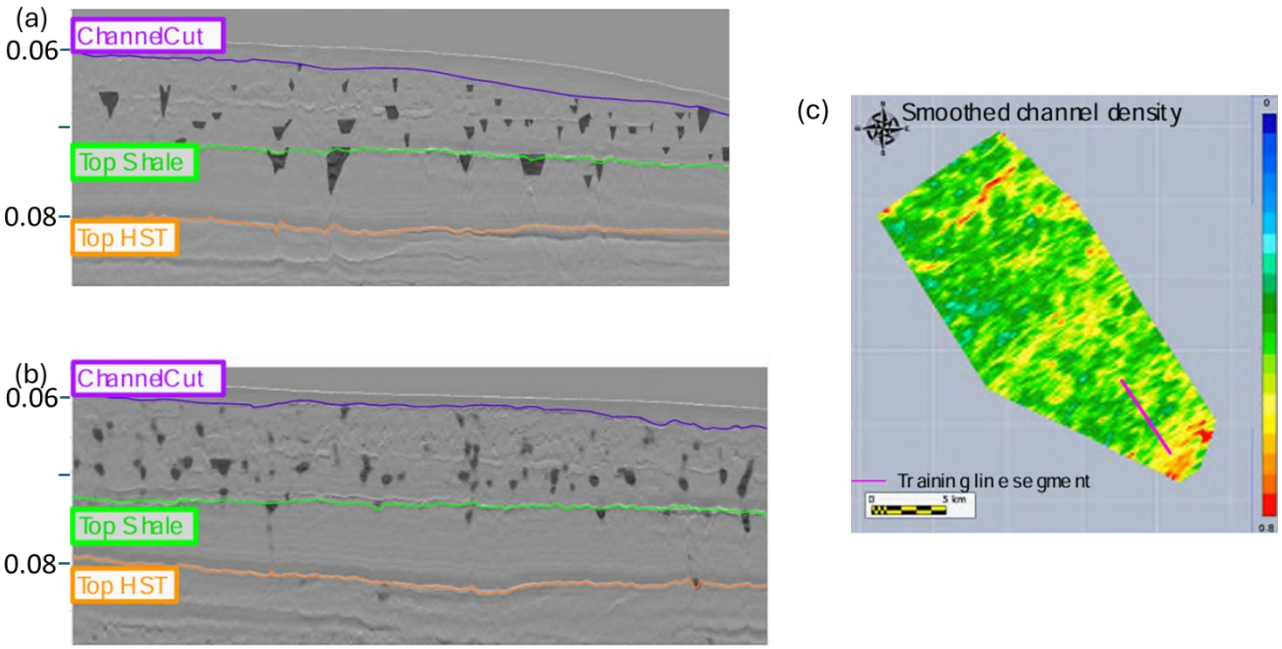

***Figure 4**: The estimation of channels using machine learning (ML) on the 2D seismic data set. (a) Line segment on which channels are identified for training of data. (b) A 2D line segment with ML identified channels with probability larger than 0.6. (c) The normalised smoothed channel density map extracted between the 'Channel Cut' and 'Top Shale' horizons. The solid magenta line shows the location of the 2D line segment used for training.*

From dense 2D seismic data to 3D seismic data interpretation

Modern interpretation tools in the oil and gas industry typically operate on 3D seismic datasets. To make use of these tools in offshore wind development, the 2D seismic data must first be transformed into a 3D volume. In our case study, where the interline spacing of the 2D data is relatively small, a dedicated kriging-based interpolation tool was developed to convert the 2D data into a 3D seismic volume.

A 3D survey grid was designed to encompass all acquired 2D lines, with seismic traces spaced at 25 meters in the inline direction and 5 meters in the

© SPG India. All rights reserved.

crossline direction, aligned with the dominant 2D acquisition orientation.

Once aligned, kriging weights were computed at each grid point, and the interpolated trace was calculated as a weighted sum of the closest input traces. Figure 5 illustrates this process. In our implementation, the kriging used a 400 m search radius, considering the 50 nearest traces for interpolation. An isotropic spherical variogram with a range of 200 m was applied to compute the kriging weights. At locations where no input traces were found within the search radius, a null trace was assigned in the 3D volume.

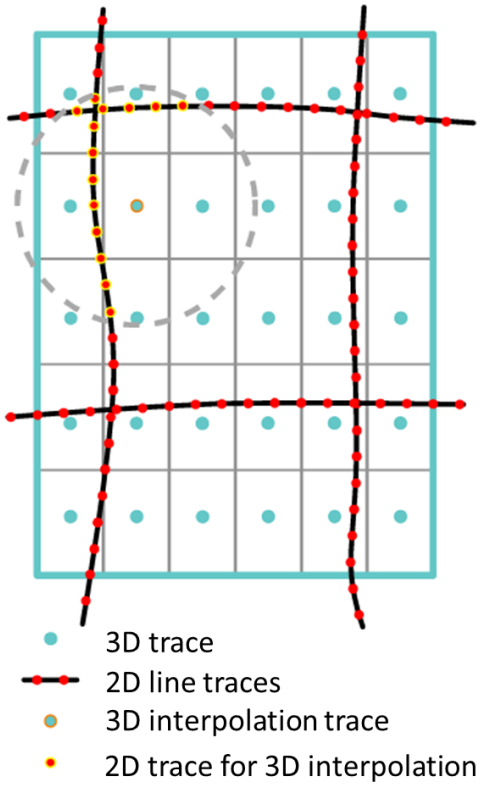

Figure 5*: The kriging-based interpolation method to arrive at a 3D seismic dataset from 2D data. For a given inline and crossline location in the 3D survey, 2D line traces are selected within the search area as indicated by the grey dashed circle. Using kriging, the trace in the 3D grid is estimated by weighted summation of the selected traces.*

Figures 6a and 6b demonstrate the fidelity of the interpolation: a section extracted from the 3D volume closely resembles the original 2D seismic line at the same location, albeit with some lateral smoothing due to the coarser (5 m) trace spacing in the 3D volume (compared to 1.5 meters in the original 2D data). While this smoothing improves the signal-to-noise ratio, it does come at the cost of some high-frequency detail. A quality control metric, the normalized standard deviation of the kriging prediction, was computed to quantify local interpolation variability (Figure 6c).

Using the processed 3D seismic volume, a Relative Geological Time (RGT) volume was computed to facilitate horizon tracking and seismic stratigraphy analysis. The RGT is computed by auto-tracking horizons from a grid of seed points using an algorithm that is developed in-house. Prior to RGT computation, the data were dip-filtered to enhance lateral coherence and aid the automatic horizon tracker. In total, 32 auto-tracked horizons were generated between the seabed and the Pleistocene Unconformity, from which 25 distinct stratigraphic layers were defined.

Next, spectral decomposition, with use of a matching pursuit algorithm (Liu and Marfurt, 2005), was performed on the data. Figure 7a shows an example of seismic line 316 with the RGT volume overlain, where layers 11 and 24 are highlighted. RGB corendering was carried out using three frequencies 200 Hz (Red), 550 Hz (Green), and 850 Hz (Blue). These frequencies were chosen to enhance the visualization of the subsurface channel features. The resulting composite images clearly delineated the channel systems. For example, Figure 7b shows Layer 11, which captures transgressive channel sands incised into estuarine deposits and trending northeast to southwest. In contrast, Figure 7c shows Layer 24, which lies below the HST sand package in Pleistocene sands, where channel orientations are more variable and complex.

To better understand lithological variations within the seismic volume, coloured inversion was computed. Unlike typical coloured inversion workflows used in hydrocarbon exploration, which emphasize impedance contrasts at higher frequencies, this inversion was tuned to enhance low-frequency content, providing greater sensitivity to variations in soil behavior types. This adjustment aids the interpretation of subsurface soil conditions relevant to foundation design

© SPG India. All rights reserved.

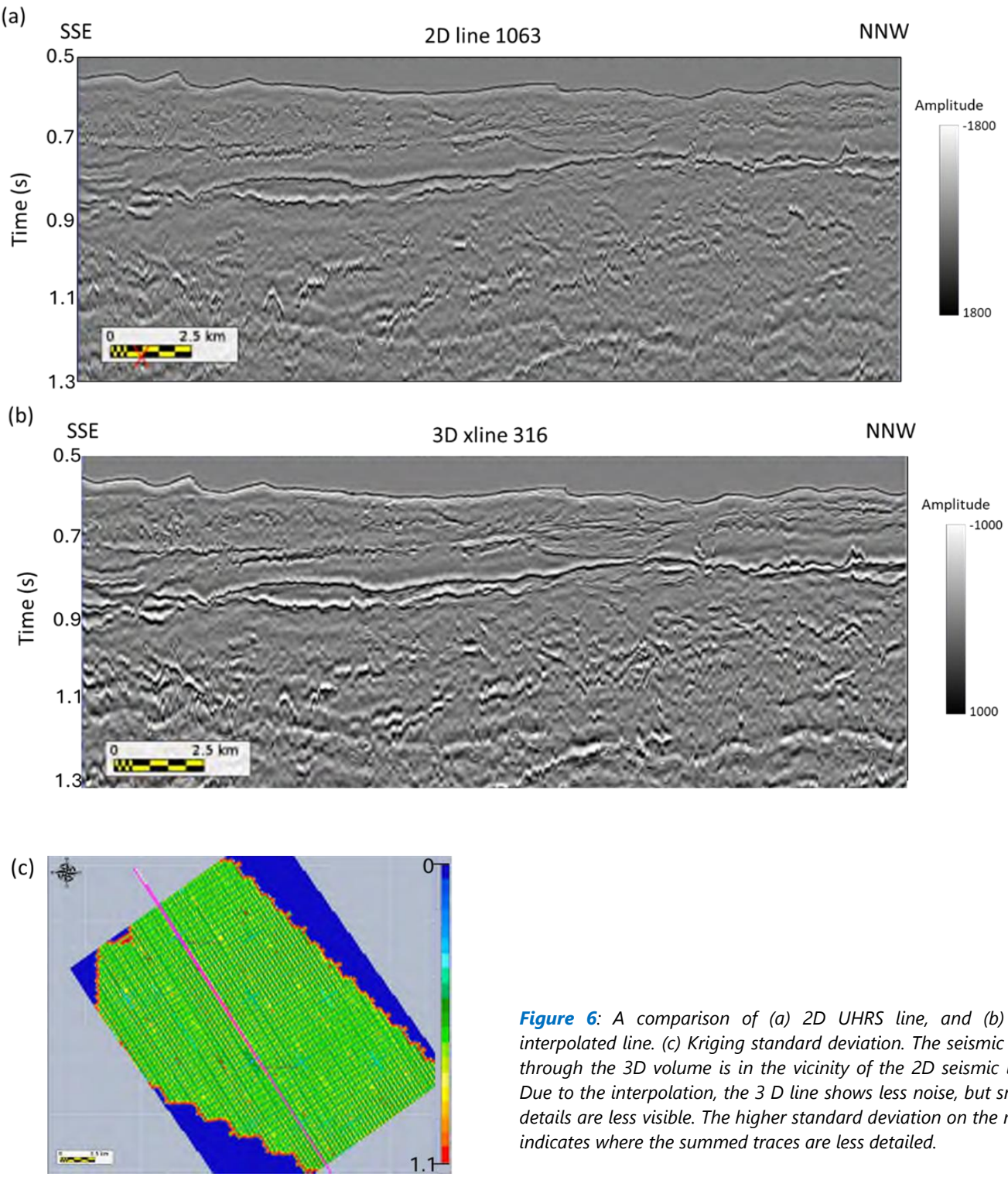

***Figure 6**: A comparison of (a) 2D UHRS line, and (b) 3D interpolated line. (c) Kriging standard deviation. The seismic line through the 3D volume is in the vicinity of the 2D seismic line. Due to the interpolation, the 3 D line shows less noise, but small details are less visible. The higher standard deviation on the map indicates where the summed traces are less detailed.*

© SPG India. All rights reserved.

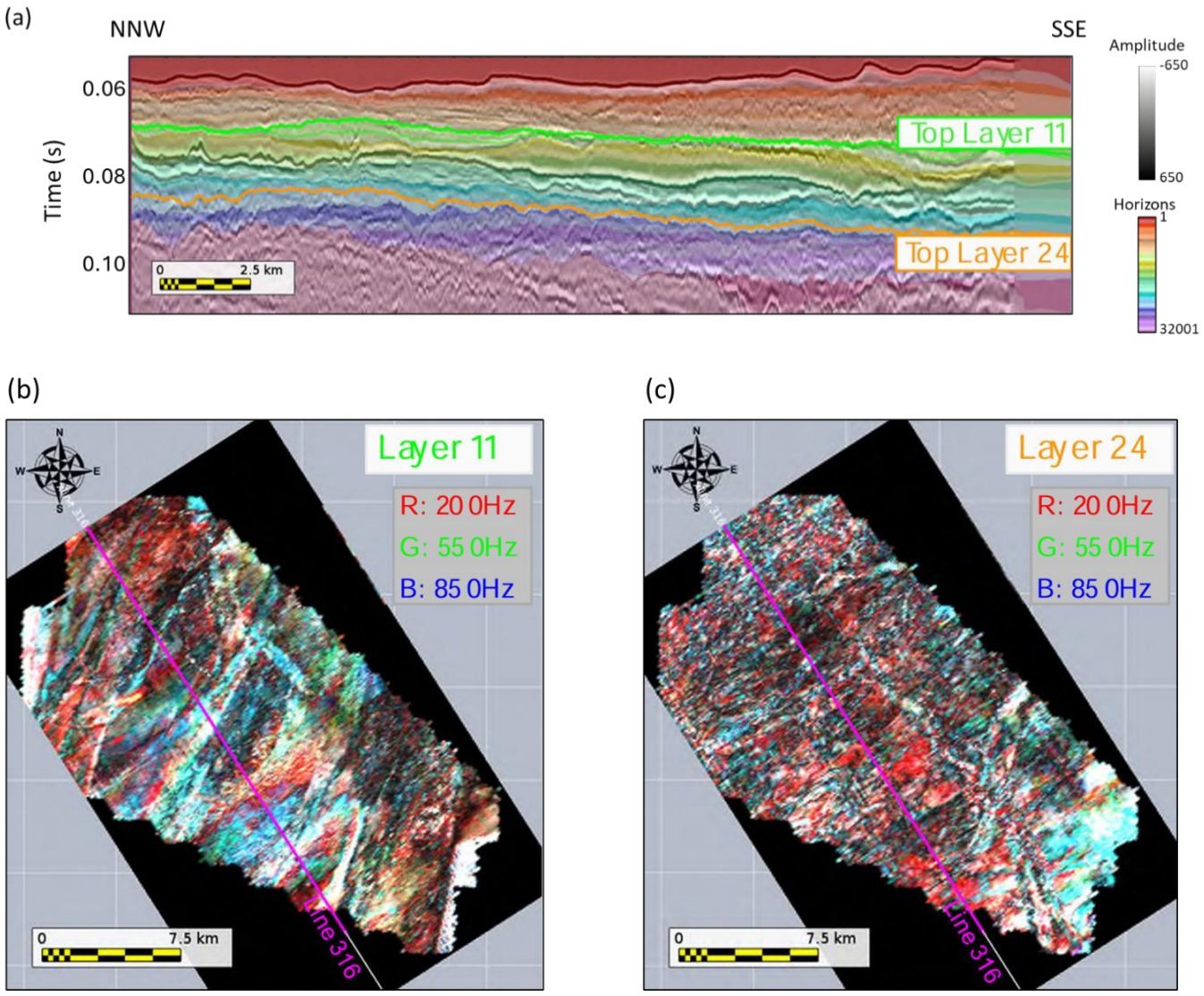

***Figure 7**: (a) A 3D seismic line display with the computed Relative Geological Time superimposed using transparency. The RGB corendered display for three spectral magnitude slices extracted along (b) layer 11, and (c) layer 24. The frequencies used in the RGB maps are 200 Hz (red), 550Hz (green) and 850Hz (blue). The spectral decomposition was computed on the 3D seismic interpolated volume using a matching pursuit algorithm.*

Well data interpretation

In hydrocarbon reservoir characterization, (electro) facies are typically identified by using several wireline log measurements. In geotechnical applications, an equivalent approach is taken with the use of the (seismic) CPT. To classify soil types, SBTs have been proposed by Robertson (2009), which relate CPT measurements to lithological interpretation.

To determine the SBT from CPT data, the tip resistance (q_t), is normalized to Q_t, using in situ vertical and effective stresses. Similarly, sleeve friction is normalized to a friction ratio (F_r). The logarithms of these two parameters are then cross-plotted on the Robertson soil classification chart (Wang et al., 2013) to identify the corresponding SBT.

Figure 8 illustrates such a cross-plot for geotechnical data acquired at Well 1. Each data point is colour-coded by burial depth, to visualize the evolution of SBT with depth. A variety of SBTs are encountered throughout the profile. Note that some of the CPT measurements at greater depths, when the CPT tool reaches its maximum penetration force limit, the data acquisition is not continuous. This necessitates the interpolation of the

© SPG India. All rights reserved.

SBT classification. The right-hand track of Figure 8 presents the interpolated SBT log, which exhibits strong agreement with the lithological log derived from borehole sampling at the same location. This interpretation workflow was systematically applied across all 10 borehole sites within the study area.

At well locations where shear wave velocity (V_S) measurements were obtained, the data were cross-plotted against burial depth for each identified SBT. These plots revealed consistent compaction trends, allowing power-law models to be fitted to the V_S versus depth relationship for the most frequently encountered SBTs, e.g. clay, sand, and sand-mixture. This modeling approach follows the methodology described by Stuyts et al. (2024).

For SBTs with limited sampling or those confined to narrow depth intervals, a global power-law model was fitted using all available V_S data, irrespective of SBT classification. Figure 9 illustrates the resulting fits, highlighting the relationship between shear wave velocity and burial depth across the full range of observed soil types.

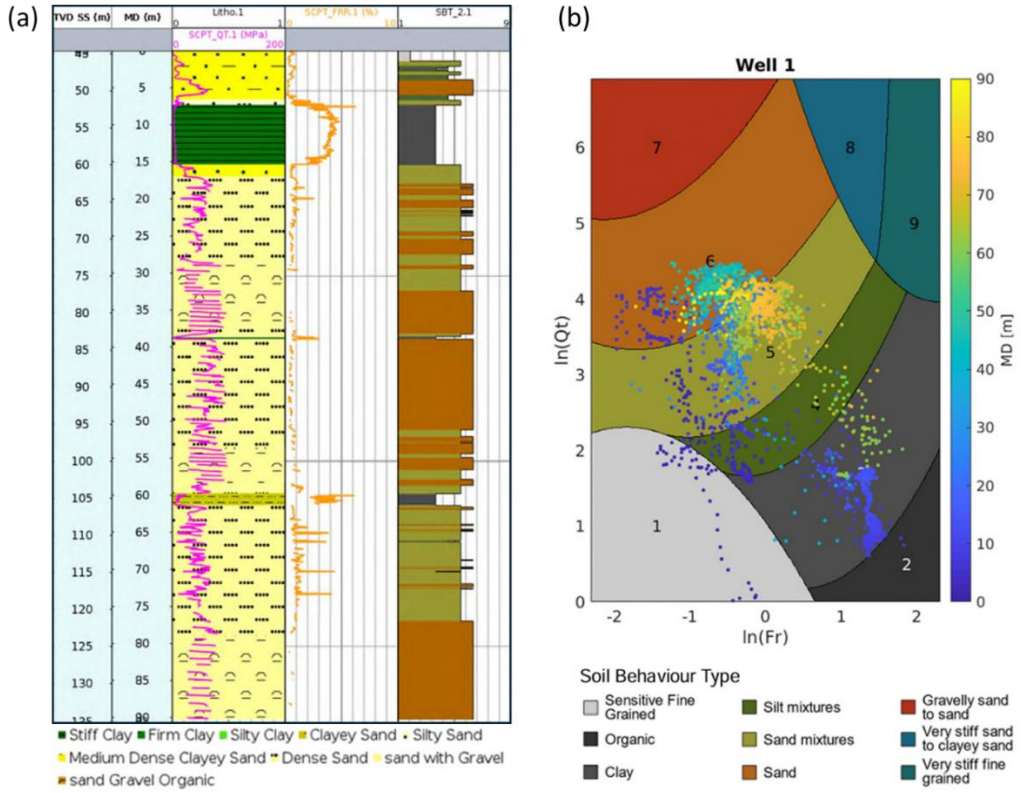

***Figure 8**: (a) Lithology log encountered in Well-1 and the computed normalized cone resistance (Q_t), and friction ratio (F_r) logs. (b) Robertson plot comprising a crossplot between ln (F_r) and ln (Q_t), with values color-coded with depth below seabed to obtain the SBT. The SBT is interpolated using lithology to arrive at a continuous SBT log shown in (a).*

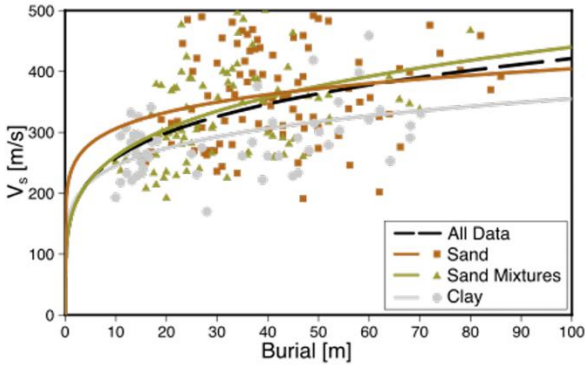

***Figure 9**: The shear wave data plotted against the burial depth for different SBT's with coloured lines representing the fitted power functions.*

SOIL FACIES AND SHEAR VELOCITY MODELLING

After preparing and interpreting the seismic data in 3D and transforming the well data into SBTs, a 3D

© SPG India. All rights reserved.

stratigraphic grid is constructed to model the distribution of SBTs. Shear wave velocity (V_S) is subsequently simulated within this grid for each SBT using established modeling techniques adapted from hydrocarbon reservoir workflows.

To construct the stratigraphic grid, the bounding seismic horizons are first converted from time to depth using the existing migration velocity model. This velocity model is interpolated into a 3D volume using the kriging method described earlier (Figure 5). At well locations, the horizons are tied directly to well markers to ensure accurate depth calibration. Between the depth-converted horizons, a stratigraphic grid is generated with square cells of 100 m by 100 m. This grid honors erosional surfaces identified during horizon interpretation and is subdivided into 10 stratigraphic units, each representing a distinct depositional environment (Figure 10a).

To better constrain the modeling within individual units, a coloured inversion is applied to the 3D interpolated seismic data. This inversion enhances lithological contrasts and is mapped onto the stratigraphic grid (Figure 10b). Within each unit, the SBTs are modeled accordingly, providing a detailed representation of subsurface soil behavior across the study area.

For each stratigraphic unit, variograms were extracted and modeled using well data to capture spatial continuity of SBTs. These variograms were validated against outcrop data and geological analogues and adjusted where necessary to reflect realistic depositional patterns. SBTs from the wells were blocked into the stratigraphic grid by assigning the dominant SBT within each cell. Geostatistical modeling was then performed for each unit using the corresponding variogram models. A total of five different geostatistical methods were applied, each selected to honor the facies proportions observed in the wells and tailored to the depositional characteristics of the unit. Specifically, indicator kriging was used for units 1 and 9, while sequential indicator kriging was applied to units 2 and 10, reflecting their distinct sedimentary architectures.



***Figure 10**: (a) The stratigraphic modelling grid constructed between the main horizons. (b) The coloured inversion transferred painted inside the modelling grid. The coloured inversion attribute is used to model SBTs with a truncated Gaussian estimation method.*

© SPG India. All rights reserved.

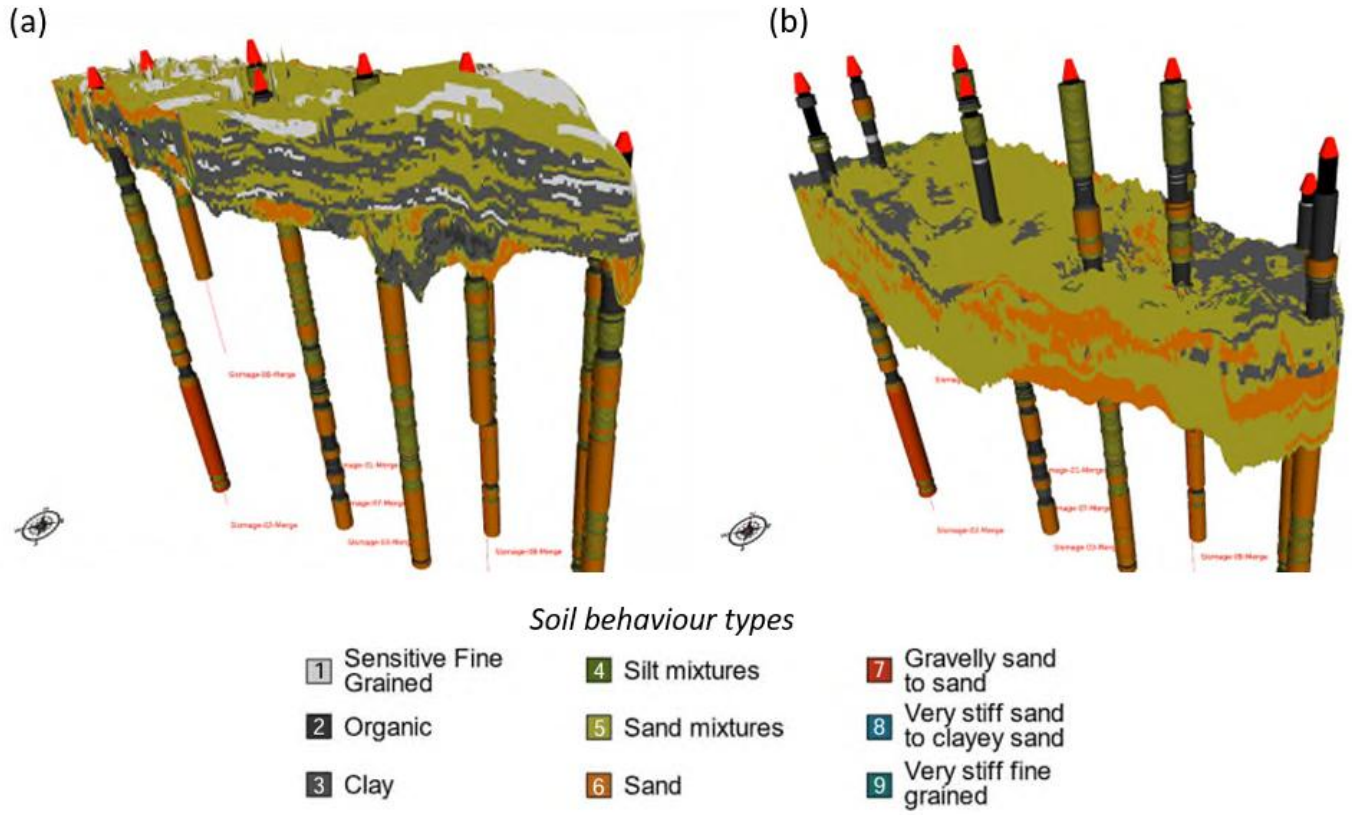

***Figure 11**: The modelled SBT facies for two stratigraphic layers, (a) In unit 3, the modelled channels are constrained by the channel density map obtained using the machine learning approach (Figure 4). (b) In unit 6, the SBT modelled using the coloured inversion as a constraint in a truncated Gaussian estimation.*

In unit 3, which represents progressive channel deposits, channels are modeled using an object-based simulation method described by Allard et al. (2006). This method simulates channel geometries and their sedimentary infill proportionally within a background matrix. The channel density map derived from Figure 4 serves as a spatial constraint, guiding the proportional distribution of channel features throughout the unit. Channel geometries and orientations are statistically modeled based on observations from layer 11 (Figure 7) and are further constrained by well data.

The resulting ensemble of models constitutes a mixed SBT facies framework, featuring two distinct channel types: one filled with sand mixtures (SBT 5), the other with clean sands (SBT 6), along with sensitive fine-grained overspill deposits (SBT 1). These are embedded within a clay-dominated background matrix (SBT 3). A realization of this channel modeling is illustrated in Figure 11a.

For the remaining stratigraphic units (4 through 8), a truncated Gaussian estimation method, as described by Biver et al. (2012), is applied. This technique simulates the most probable facies distributions based on auxiliary data. Within each unit, a random Gaussian field is generated, and the likely facies are determined using a truncated Gaussian technique.

To model the SBTs encountered in these units, the coloured inversion results (Figure 10b) are used as constraints. The lithology values are derived by mapping the uniform transform of the coloured inversion onto the probability of occurrence of each facies, as defined by the well data. By simulating a 3D Gaussian random field within the grid and applying truncation on the probability distribution function, the SBT distribution is generated. Different variogram models are used across the units to capture the geological variability.

Figure 11b shows a model realization of the truncated Gaussian simulation for unit 6. The complete 3D SBT

© SPG India. All rights reserved.

model combining all units is displayed in Figure 12a. Within the suite of 3D SBT models, shear wave velocities are co-simulated using the power-law relationships established earlier (Figure 9), resulting in a family of shear wave velocity models.

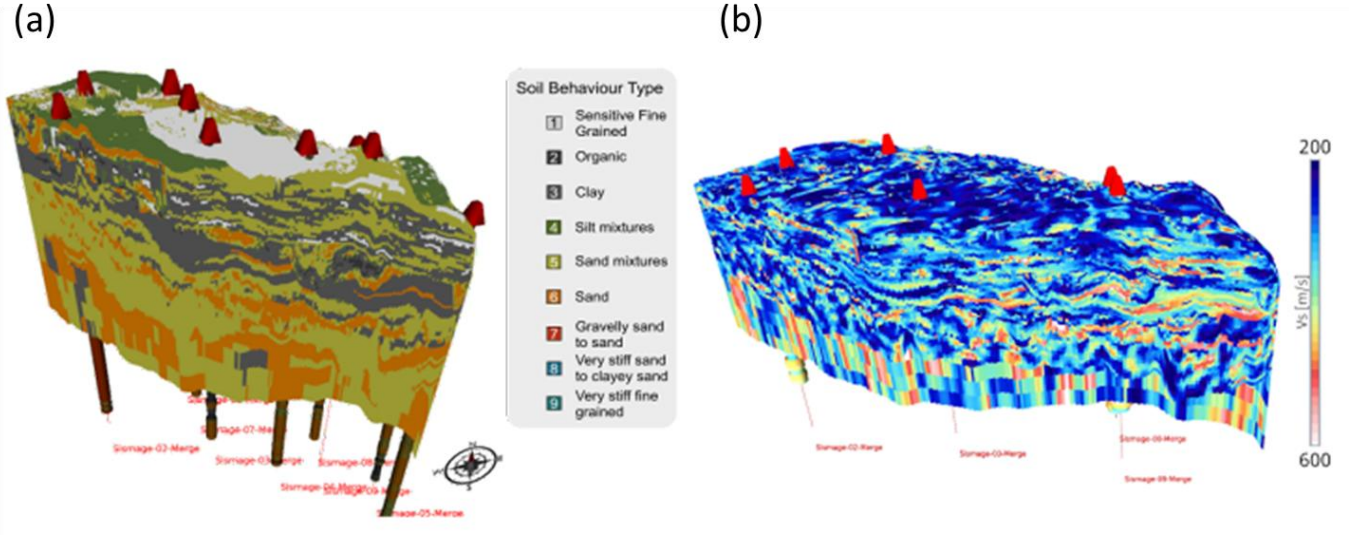

***Figure 12**: a) A single simulation of the SBT model. b) A co-simulated shear velocity model. For each SBT in the model, a shear velocity is modelled. Together with the density the small-scale shear strength can be derived from the model.*

CONCLUSIONS

This paper investigates how geotechnical data collected for windfarm soil characterization can be adapted for use with hydrocarbon reservoir modeling techniques. Applying these methods to the adapted dataset enhances the evaluation of shallow subsurface conditions, supporting the initial selection of wind turbine foundation-to-soil coupling functions.

The data collected for windfarm development include individual boreholes and 2D UHRS surveys. Borehole data are transformed into SBTs to support geological modeling of the shallow subsurface. Power-law relationships capture the increase in shear wave velocity with burial depth for different SBTs. For interpretation of individual 2D seismic lines for channels, machine learning techniques help identify channels, and produce a channel density map. Additionally, specialized kriging methods convert the dense 2D data into a 3D seismic volume. Interpretation of the 3D volume using Relative Geological Time and spectral decomposition further improves geological understanding. A 3D depth model of SBTs is constructed using various reservoir modeling techniques applied to different stratigraphic layers. Shear wave velocity is co-simulated for each SBT within the model. This modeling sequence is repeated multiple times to generate a family of models. When soil bulk density is known, the desired small-scale shear strength and its associated uncertainty can be extracted for any potential wind turbine location.

The proposed methodology is accurate and should be adopted for more such exercises.

ACKNOWLEDGEMENTS

The authors gratefully acknowledge the management of TotalEnergies for granting permission to publish this methodology. All the interpretation and modelling are performed using our in-house geoscience software package Sismage-CIG. We also sincerely thank the reviewers for their valuable feedback, which greatly improved the clarity and accessibility of the manuscript.

REFERENCES

Allard, D., R. Froidevaux, and P. Biver, 2006, Conditional simulation of multi-type nonstationary Markov object models

© SPG India. All rights reserved.

respecting specified proportions, Math. Geol., **38**, no. 8, 959–986. https://doi.org/10.1007/s11004-006-9057-5

Arany, L., S. Bhattacharya, J. Macdonald, and Hogan, J., 2017, Design of monopiles for offshore wind turbines in 10 steps, Soil Dynamics and Earthquake Engineering, **92**, 126–152. https://doi.org/10.1016/j.soildyn.2016.09.024

Biver, P., F. Pivot, V. Henrion, 2012, Estimation of most likely lithology map in the context of Truncated Gaussian techniques, Ninth International Geostatistics Congress, Oslo, Norway, 11-15.

Cazzaro, D., A. Trivella, F. Corman, and D. Pisinger, 2022, Multi-scale optimization of the design of offshore wind farms, Applied Energy, **314**, 118830. https://doi.org/10.1016/j.apenergy.2022.118830

Damgaard, M., M. Bayat, L. V. Andersen, and L. B. Ibsen, 2014, Assessment of the dynamic behaviour of saturated soil subjected to cyclic loading from offshore monopile wind turbine foundations, Computers and Geotechnics, **61**, 116-126. https://doi.org/10.1016/j.compgeo.2014.05.008

Lombardi, D., S. Bhattacharya, and D. M. Wood, 2013, Dynamic soil-structure interaction of monopile supported wind turbines in cohesive soils, Soil dynamics and Earthquake Engineering, **49**, 165-180. https://doi.org/10.1016/j.soildyn.2013.01.015

Murphy, G., D. Igoe, P. Dohorty and K. Gavin, 2018, 3D FEM approach for laterally loaded monopile design, Computers and Geotechnics, **100**, 76-83. https://doi.org/10.1016/j.compgeo.2018.03.013

Robertson, P. K. 2009, Interpretation of cone penetration tests—a unified approach, Canadian Geotechnical Journal, **46**, no. 11, 1337-1355. https://doi.org/10.1139/T09-065

Stuyts, B. Weijtjens, W., Sastre Jurado, C. Devriendt, C. and Kheffache, A., 2024, A Critical Review of Cone Penetration Test-Based Correlations for Estimating Small-Strain Shear Modulus in North Sea Soils, Geotechnics, **4**(2), 604-635. https://doi.org/10.3390/geotechnics4020033

Vieira, M., B. Snyder, E. Henriques, and I. Reis, 2019, European offshore wind capital cost trends up to 2020, Energy Policy, **129**, 1364-1371. https://doi.org/10.1016/j.enpol.2019.03.036

Wang, Y., K. Huang, and Z. Cao, 2013, Probabilistic identification of underground soil stratification using cone penetration tests, Canadian Geotechnical Journal, **50**, 766-776. https://doi.org/10.1139/cgj-2013-0004

BIOGRAPHIES



Leon Barens is a senior geophysicist. He holds a master's in mining engineering from Delft University of Technology, a Mastère Specicialisé in Reservoir management from IFP school in Paris and a Ph.D. from Heriot Watt University in Petroleum Engineering. He worked briefly for Schlumberger as a wireline engineer in between studies. After his Ph.D. he worked for TotalEnergies in research, exploration and field development. He strives to find innovative methods to improve and accelerate seismic data interpretation and reservoir characterisation.



Khalid Tarek is a senior geophysicist. He has a master's in reservoir engineering at ENSAM (Ecole National supérieur d'Arts et Métier) and another master's degree in exploration geophysics from University of Pau.

© SPG India. All rights reserved.



Julien Lalanne is a Ph.D. student at Laboratoire Navier - École Nationale des Ponts et Chaussées and TotalEnergies, working at the intersection of generative modeling and geosciences. Prior to his Ph.D., he worked as a research engineer at TotalEnergies, where he developed machine learning methods for seismic and well log data analysis. He holds a master's in applied mathematics from Université Grenoble Alpes and an engineering degree from Grenoble INP – Ensimag.



Eric Cauquil is an expert on site investigation and geohazard assessment. He holds a Ph.D. in Earth Science from Paris-Sorbonne University. He has been and is project manager of several R&D and innovation initiatives to improve and leverage geohazard assessment strategies for both oil and gas and offshore windfarm projects.

Geo Snap



Overturned folds in Paleozoic Kanawar and Kuling Group rocks in Pin Valley, Spiti-Zanskar Basin.

(Photo courtesy: Syed Shadab Ahmed and Deepak Rawat, ONGC)

© SPG India. All rights reserved.